



Inner filter effect-based highly sensitive quantification of 4-nitrophenol by strong fluorescent N, S co-doped carbon dots

Kandasamy Sasikumar¹ · Ramar Rajamanikandan¹ · Heongkyu Ju¹

Received: 3 October 2023 / Revised: 25 November 2023 / Accepted: 29 November 2023 / Published online: 4 January 2024
© The Author(s), under exclusive licence to Korean Carbon Society 2024

Abstract

4-Nitrophenol (4NP) is a vital intermediate in organic industries, and its exploitation creates serious environmental issues. We propose a fluorescence quenching-based strategy with nitrogen and sulfur co-doped carbon dots (NS-CDs) for highly sensitive 4NP detection with excellent selectivity. The NS-CDs are produced through the hydrothermal process, in which citric acid serves as a carbon source and cysteamine hydrochloride as a source of N and S. The effect of doping was also studied by synthesizing undoped CDs and examining their properties. As-developed NS-CDs exhibit a bright cyan blue color with maximum emission centered at 465 nm. The fluorescence of NS-CDs is significantly quenched in an approximately linear fashion with increasing 4NP concentration (7.5–97.5 μM). The inner filter effect (IFE) and static quenching (SQ) between NS-CDs and 4NP are responsible for such fluorescence reduction. The fluorimetry technique enables the quantification of 4NP with a limit of detection (LOD) of about 0.028 μM . Moreover, the fluorescence quenching is tested for several other chemical compounds but they generate false quenching signals; only 4NP leads to fluorescence quenching of NS-CDs, demonstrating excellent selectivity. The “turn-off” fluorescence properties and visually apparent color change of the fluorescent probe reveal the excellent performance for 4NP sensing. The NS-CDs’ capability of quantifying 4NP in real water samples (tap water and drinking water) produces an excellent recovery rate ranging between 96.24 and 98.36%.

Keywords 4-Nitrophenol · Carbon dots · Cysteamine hydrochloride · HR-TEM · Inner filter effect · Nitrogen and sulfur co-doping

1 Introduction

4-Nitrophenol (4NP), an aromatic phenolic compound, is an inevitable intermediate in manufacturing numerous organic products [1]. The exploitation of 4NP for the massive production of drugs (paracetamol) and pesticides (parathion, fenitrothion), however, has unwanted consequences of its continuous dissemination in aquatic and soil environments. 4NP, one of the perilous chemical pollutants, persists in the environment for a long period due to its high stability, extreme water solubility, acute toxicity, and poor biodegradability [2]. High-level ingestion of 4NP can interfere with hemoglobin in human blood and turn it into methemoglobin (the condition called “methemoglobinemia”). The symptoms of the disease may include headache, fatigue,

dizziness, nausea, and cyanosis (blue-colored skin and lips). Moreover, it can irritate and burn human skin and eyes with possible eye damage. Its continuous and repeated exposure can also affect the respiratory and nervous systems [3, 4]. Unless treated with care and disposed of appropriately, 4NP would cause a foul environment. As per the Environmental Protection Agency (EPA) guidelines, the maximum acceptable level of 4NP in drinking water is less than 0.43 μM [3]. Hence, it is crucial to develop a rational and efficient analytical technique for rapidly quantifying trace 4NP in the environment, especially in water bodies.

The analytical techniques currently available for quantification of 4NP in water include those based on spectrophotometry, electrochemical, capillary electrophoresis, high-performance liquid chromatography (HPLC), and gas chromatography [5–9]. These methods, however, frequently encounter challenges such as electrode instability, time-consuming preparation procedures, expensive and sophisticated instrumentation, and difficulties in rapid assay. In contrast, fluorimetry-based sensing offers several benefits such as

✉ Heongkyu Ju
batu@gachon.ac.kr

¹ Department of Physics, Gachon University, Seongnam-si, Gyeonggi-do 13120, Republic of Korea

superior sensitivity, selectivity, operational simplicity, real-time/in-situ detection, minimal sample requirement, and high reproducibility.

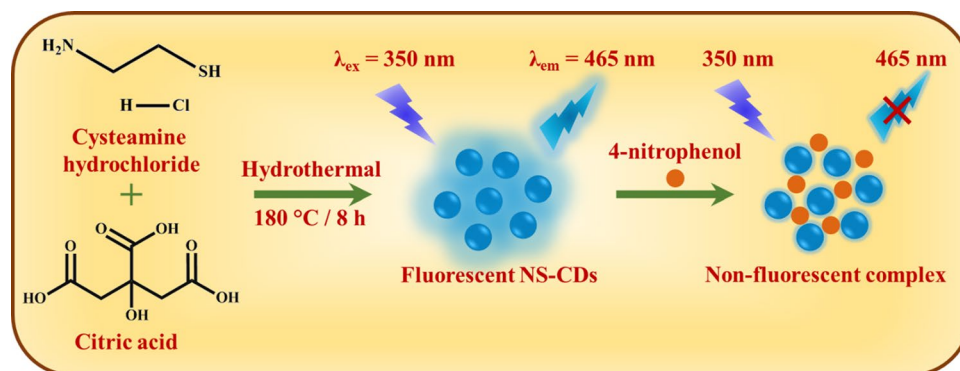
Carbon nanomaterials have been widely researched in the past few years due to their interesting properties [10–14]. Carbon dots (CDs) are novel nanomaterials with sizes typically less than 10 nm. Owing to their biocompatibility, ease of synthesis, low toxicity, diverse surface functionalization, tunable photoluminescence, uncompromising chemical stability, and photostability, CDs have garnered extensive attention in the prospective applications of optoelectronics, biomedicine, bioimaging, sensing, and catalysis [15–18]. Besides, their fascinating fluorescence properties have enabled them to be used as fluorescent probes for detecting various substances, including metal ions and pollutants in the environment [19]. The fluorescence characteristics of CDs are affected by several factors, including the carbonaceous core structure, dopants, impurities, surface functional groups, and organic fluorophores produced as a byproduct of synthesis [20]. The chemical structure of CDs can be altered by choice of carbon precursor and synthesis method. CDs have been synthesized from a variety of precursors via laser ablation, chemical vapor deposition, hydrothermal, and microwave-assisted techniques [21–24].

In hydrothermal synthesis, the precursors for CDs could be graphite or graphene-like polycyclic aromatic hydrocarbons, organic acids, polysaccharides, organic wastes, biopolymers, and other natural carbon sources [25]. Different precursors could lead the synthesized CDs to have different core structures with either pure *sp*²-hybridized carbon or a combination of *sp*² and *sp*³-hybridized carbon [26]. According to recent reports, doping heteroatoms like nitrogen (N), sulfur (S), boron (B), and phosphorus (P) can be a simple and effective way to boost the optical and electronic characteristics of CDs [27]. For instance, n-type doping, which involves the incorporation of N or S, could enhance the electron density over the CDs' surface, resulting in a high quantum

yield (QY) [28, 29]. In addition, the doping allows many functional groups to be further attached over the CDs' surface, leading to bandgap-dependent multicolor emission [30]. The newly formed surface states on the carbon core can also result in excitation-independent emission properties. The use of cysteamine hydrochloride is found to be an effective means for heteroatom co-doping due to the existence of both amine (–NH₂) and thiol (–SH) functional groups in its molecule [31, 32]. Thus, cysteamine-based doping could enrich the fluorescence properties of CDs through the synergistic effect of N and S heteroatoms co-doped in CDs (NS-CDs). Earlier, NS-CDs were synthesized via microwave-assisted pyrolysis of cysteamine hydrochloride and ammonium citrate for quantification of ascorbic acid and chromium (VI) [33]. The NS-CDs displayed a QY of up to 54.8% and strong photostability. Citric acid monohydrate and cysteamine were exploited to produce NS-CDs for the applications of Cr₂O₇²⁻ and Fe(CN)₆³⁻ detection, cell imaging, and fluorescent composite films [34].

In this paper, we reported the fluorescent NS-CDs synthesized through a single-step hydrothermal strategy using low-cost precursors, citric acid (CA) and cysteamine hydrochloride, in water (Scheme 1). C-CDs were prepared using citric acid only. The –OH, –COOH, and –NH₂ groups attached to the carbon core facilitated the good dispersion of NS-CDs in water. The as-produced cyan blue emissive NS-CDs exhibited a high QY of about 52%, robustness to photobleaching, and good photostability. The NS-CDs fluorescent probe allowed for the sensitive and selective quantification of 4NP with a LOD of 0.028 μM through its fluorescence quenching upon 4NP addition; the inner filter effect (IFE) and (SQ) process were the main drives for quenching. The results indicate that the NS-CDs fluorescent probe can find an effective application in the quantitative detection of 4NP in tap water and drinking water.

Scheme 1 Synthesis route of fluorescent NS-CDs and 4NP sensing



2 Experimental

2.1 Chemicals

Citric acid, phenol, p-phenylenediamine (pPD), 2-nitrotoluene (2NT), aniline, 4-nitroaniline (4NA), 4-chloroaniline (4CA), 4-bromophenol (4BP), 4-nitrophenol (4NP), 3-nitrophenol (3NP), 2-nitrophenol (2NP), 4-nitrobenzoic acid (4NBA), and hydroquinone (HQ) were procured from Sigma Aldrich. Cysteamine hydrochloride was provided by Acros Organics. All the reagents were directly used since they were analytical grade. All the experiments were conducted using ultrapure water.

2.2 Synthesis of NS-CDs

In a typical synthesis of NS-CDs, 0.1 M citric acid (0.77 g, C₆H₈O₇) was weighed and dissolved in 20 mL water. With this solution, 0.2 M cysteamine hydrochloride (1.80 g, C₂H₇NS·HCl) dissolved in 20 mL water was mixed under vigorous stirring. This reaction mixture (net volume of 40 mL) was shifted to a Teflon-lined autoclave vessel (volume of 50 mL) and permitted to a hydrothermal reaction at 180 °C temperature for 8 h. The obtained solution was naturally cooled to room temperature, centrifuged at 10,000 rpm for 30 min, and then dialyzed with a dialysis bag (molecular weight cut-off: 500 Da) for 48 h. Finally, the product was freeze-dried to obtain NS-CD powder for further use. For comparison, CDs were prepared without cysteamine under identical hydrothermal conditions, and were marked as C-CDs.

2.3 Instrumentation

Fourier transform-infrared (FT-IR) spectral analysis was carried out on a JASCO FT-IR/4600 spectrophotometer. UV–Vis absorption spectra were measured on a JASCO V/770 spectrophotometer. Fluorescence spectral measurements were performed on SCINCO FS/2 fluorescence spectrometer. Raman spectrum was acquired using the Ramboss 500i Micro Raman system with a 633 nm He–Ne laser source. High resolution-transmission electron microscopic (HR-TEM) photographs of NS-CDs coated over a carbon grid were taken on a Tecnai G2 F30, FEI instrument at an operating voltage of 300 kV. X-ray photoelectron spectroscopy (XPS) was performed using a Thermo Scientific VG multiLab/2000 instrument with a monochromatic Al K_α source. Fluorescence lifetime experiments were conducted on a time-correlated single

photon counting (TCSPC) instrument (DeltaPro, Horiba Scientific) equipped with a 390 nm excitation laser.

2.4 Quantum yield (QY) measurement

To measure the QY of NS-CDs, quinine sulfate dissolved in 0.1 M H₂SO₄ (QY = 54% at 360 nm excitation) was used as a reference. The QY was calculated using the equation [35],

$$QY_S = QY_R \frac{I_S A_R}{I_R A_S} \left(\frac{n_S}{n_R} \right)^2, \quad (1)$$

where QY, *I*, *A*, and *n* are the quantum yield, the integrated intensity, the absorbance, and the refractive index, respectively. The “S” and “R” denote the sample and reference. Since NS-CDs and quinine sulfate were prepared in ultrapure water both *n_S* and *n_R* values were taken as 1.33. The absorbance was kept below 0.05.

2.5 Analytical procedure for the 4NP detection

4NP was successfully detected in a 100% aqueous solution. The appropriate amount of 4NP ranging from 7.5 to 97.5 μM was sequentially added to 0.5 mL of NS-CDs probe solution in a standard measuring flask, and the final volume was corrected to 5 mL with ultrapure water. Next, this reaction mixture was incubated for 3 min and the fluorescence spectrum was recorded at the excitation wavelength of 350 nm. A similar process was followed to appraise the selectivity of NS-CDs to 4NP among various interfering agents such as phenol, p-phenylenediamine (pPD), 2-nitrotoluene (2NT), aniline, 4-nitroaniline (4NA), 4-chloroaniline (4CA), 4-bromophenol (4BP), 2-nitrophenol (2NP), 3-nitrophenol (3NP), 4-nitrobenzoic acid (4NBA), and hydroquinone (HQ). The same procedure was taken for C-CDs with the concentration of 4NP in the range of 10–400 μM. All the measurements were repeated five times for each analyte.

2.6 Analysis in real water samples

To quantify 4NP in real water samples, tap water and drinking water samples were first collected in glass vessels and they were immediately subjected to analysis without any pretreatments. Both water samples were spiked with known concentrations of 4NP (25 and 50 μM) and were used for the quantification of 4NP via the fluorescence quenching of NS-CDs. A known concentration of the 4NP-spiked water sample was added to NS-CDs and shaken well. After 3 min incubation time, emission spectral measurements were performed in the wavelength range of 380–580 nm with an

excitation of 350 nm. The recovery (%) was estimated from the equation [36],

$$\text{Recovery (\%)} = \frac{\text{Detected 4NP}}{\text{Spiked 4NP}} \times 100. \quad (2)$$

3 Results and discussion

3.1 Analysis of morphology and surface functional groups

The morphology and size of NS-CDs were characterized by TEM and HR-TEM, respectively. Figure 1a, b shows the NS-CDs at different magnifications. The as-synthesized NS-CDs were ultra-small and almost spherical-shaped with good dispersibility. Conversely, the fresh CDs prepared without N, S doping (C-CDs) had a non-uniform distribution and the C-CDs aged for 14 days displayed an agglomerated structure as seen in the TEM images in Fig. S1a, b. In Fig. 1b, the HR-TEM image supports better crystallinity of NS-CDs.

As seen in the inset of Fig. 1c, due to the doping of N and S heteroatoms in the CD's structure, the lattice spacing has become slightly larger (0.27 nm) than the (1120) lattice spacing (0.24 nm) of graphene [37]. The size distribution of particles was calculated from the TEM image (with a minimum of 100 particles) shown in Fig. 1a. As shown in Fig. 1d, the diameter of NS-CDs varied between 1.8 and 4 nm, and the mean diameter was about 2.81 nm.

The NS-CDs were characterized by XPS to investigate the chemical properties and surface compositions. In Fig. S2, the XPS survey scan demonstrates four characteristic peaks at 166.28 eV, 284.40 eV, 400.78 eV, and 531.69 eV, corresponding to S 2p, C 1s, N 1s, and O 1s, respectively. As displayed in Fig. 2a, the C 1s spectrum of NS-CDs is resolved into three peaks at 288.50 eV, 286.26 eV, and 284.84 eV, which can be assigned to C=O, C–N/C–O, and C=C/C–C bonding, respectively [38–41]. The O 1s spectrum in Fig. 2b can be deconvoluted into two main peaks at 533.02 eV and 531.48 eV corresponding to C=O and C–O–C/C–OH, respectively. The N 1s spectrum in Fig. 2c clearly exhibits two main peaks at 400.89 eV and 399.48 eV associated with C–N–C and N–H, respectively

Fig. 1 a TEM and b HR-TEM photographs of NS-CDs. c HR-TEM photograph of NS-CDs. The inset displays the single NS-CD's lattice. d Size distribution of NS-CDs

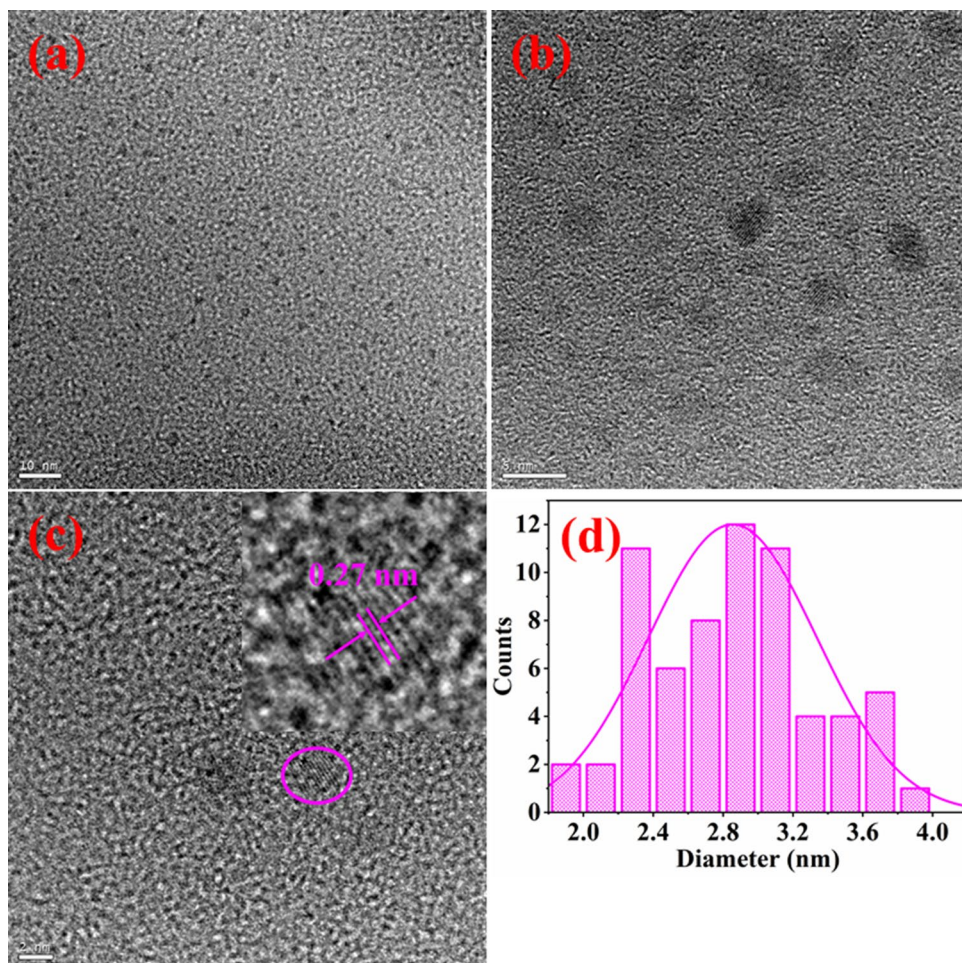
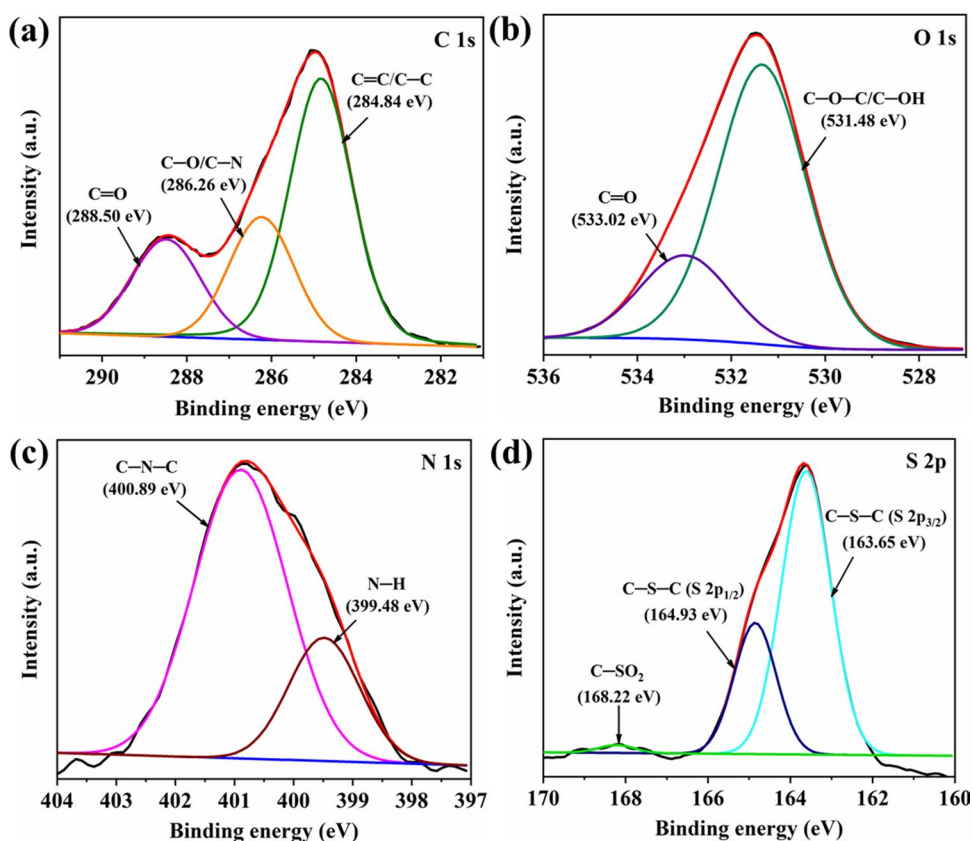


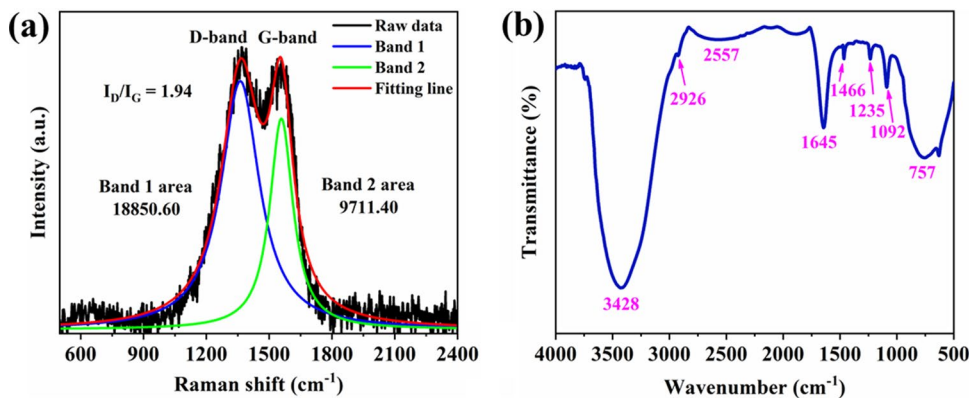
Fig. 2 High-resolution **a** C 1s, **b** O 1s, **c** N 1s, and **d** S 2p peaks of NS-CDs



[42]. In Fig. 2d, the high-resolution S 2p spectrum consists of three peaks at 168.22 eV, 164.93 eV, and 163.65 eV. The peak at higher energy represents the presence of C-SO_x sulfone bridges while the other two peaks correspond to S 2p_{1/2} and S 2p_{3/2} spectra of the C-S-C covalent bond in a thiophene-type structure due to the spin-orbit splitting [43, 44]. Accordingly, C-CDs were taken to XPS to identify their elemental compositions and molecular structure. As shown in Fig. S2b, only C and O elements are present in C-CDs. The C 1s spectrum in Fig. S2c shows the binding energies of 287.88 eV, 286.58 eV, and 284.90 eV for C=O, C-O, and C=C/C-C groups, respectively. In Fig. S2d, the O 1s

spectrum is deconvoluted into 532.86 eV and 530.99 eV, which corresponds to the C=O and C-O-C/OH groups, respectively [38, 42]. Raman spectral analysis was also performed to study the structural properties of NS-CDs. As seen in Fig. 3a, the Raman spectrum exhibits two distinct characteristic bands near 1362 cm⁻¹ (D-band) and 1559 cm⁻¹ (G-band) related to the disorder-induced vibration modes of the sp³-hybridized graphitic carbon and the in-plane vibration modes of sp²-hybridized graphitic carbon, respectively [45–48]. The areal ratio (I_D/I_G) is 1.94, signifying the low degree of graphitization and the existence of

Fig. 3 **a** Raman spectrum and **b** FT-IR spectrum of NS-CDs



disordered carbon. The result well agrees with the HR-TEM and XPS results of NS-CDs.

The surface functional groups of NS-CDs were reported by FT-IR spectrum. As shown in Fig. 3b, the characteristic absorption band centered at 3428 cm^{-1} was due to the N–H and/or OH groups. The sharp peak at 2926 cm^{-1} was related to the C–H stretching vibrations [33]. The peak positioned at 2557 cm^{-1} was due to the S–H bending vibrations [49]. Two peaks located at 1645 cm^{-1} and 1466 cm^{-1} arose due to the C=O and C–N stretching vibrations, respectively [33, 50]. The absorption peak at 1235 cm^{-1} was attributed to the C–O stretching vibrations, and another peak at 1092 cm^{-1} could be ascribed to the C–O and C–S stretching vibrations [33, 34]. The peak at 757 cm^{-1} was due to the C–S stretching vibrations [49]. Similarly, the FT-IR spectrum of C-CDs in Fig. S3a shows the absorption band at 3418 cm^{-1} due to the OH groups. The peak at 1645 cm^{-1} corresponded to the C=O stretching vibrations. The absorption peaks at 1231 cm^{-1} and 1091 cm^{-1} were attributed to the C–O stretching vibrations. The peak at 769 cm^{-1} was due to the C–H stretching vibrations, confirming the formation of C-CDs without N and S dopants.

3.2 Optical properties

The optical properties of the produced NS-CDs were studied through the UV–Vis absorption and fluorescence spectral measurements. As seen in Fig. 4a, the absorption spectrum of NS-CDs clearly shows a small hump at around 246 nm associated with π – π^* transition of the aromatic sp^2 domains. The additional peak located at 342 nm was due to the trapping of excited-state energy by the surface states, resulting in strong emission [51]. For the excitation at 350 nm, the emission peak was clearly observed at 465 nm. In addition,

the inset photographs of Fig. 4a show the deep yellow NS-CDs solution in daylight, generating a bright cyan blue light under UV irradiation at $\lambda_{UV} = 365\text{ nm}$, which could be clearly viewed by the naked eye. For C-CDs, the absorption peak was observed at 340 nm (Fig. S3b). Moreover, the relative QY of purified NS-CDs was determined at 350 nm. They displayed a high QY of about 52%, signifying the strong fluorescence in UV light. But the QY was only 18% for C-CDs. The NS-CDs display excellent QY compared to C-CDs.

The emission spectrum of NS-CDs was recorded in the wavelength range of 380–580 nm under different excitation wavelengths. As seen in Fig. 4b, the emission of NS-CDs was independent of the excitation wavelength. With the increase of excitation wavelength from 325 to 375 nm, the emission intensity initially increased and then decreased. The emission intensity was maximum for the excitation at 350 nm and the emission wavelength of NS-CDs was almost unchanged and centered at $\sim 465\text{ nm}$. This excitation wavelength-independent emission behavior is mainly due to the uniform surface states created by the functional groups attached to the carbon core and homogeneous structure.

3.3 Photostability of NS-CDs

The fluorescence stability was investigated for the NS-CDs in different time intervals under UV light. The as-prepared NS-CDs were continuously exposed to UV light ($\lambda_{UV} = 365\text{ nm}$) for 120 min duration. As displayed in Fig. 5a, there was no change in the fluorescence spectrum after long time UV exposure, demonstrating the exceptional photostability of NS-CDs. But, the fresh C-CDs (without N, S doping) showed comparatively poor photostability in UV light. As seen in Fig. S4a, the initial fluorescence intensity

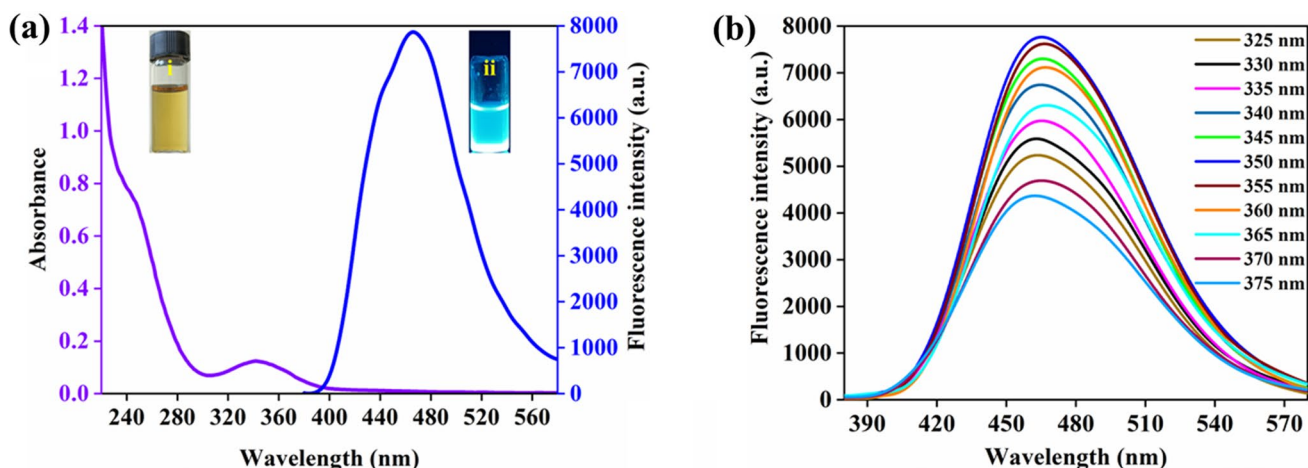


Fig. 4 **a** UV absorption and emission spectra of NS-CDs. The insets are the photographs of the newly prepared NS-CDs in (i) daylight and (ii) UV light ($\lambda_{UV} = 365\text{ nm}$). **b** Emission spectra of NS-CDs under different excitation wavelengths

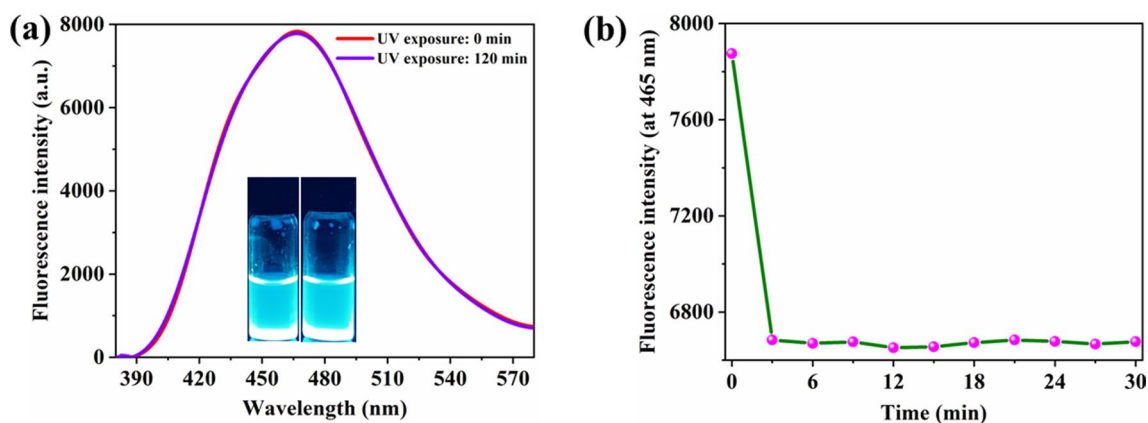


Fig. 5 **a** Photostability of NS-CDs exposed in UV light ($\lambda_{UV}=365$ nm) for 120 min. The inset displays the corresponding photographs of NS-CDs. **b** Influence of time on the fluorescence of NS-CDs after the 4NP addition ($7.5 \mu\text{M}$)

was moderately reduced after 120 min of UV exposure. Further, the C-CDs displayed less fluorescence after 14 days of aging as noticed in Fig. S4b, showing the poor storage stability of C-CDs. Interestingly, NS-CDs showed outstanding stability, which persisted even after they were aged for 2 months. The influence of incubation time on the fluorescence intensity of NS-CDs was studied. As seen in Fig. 5b, the fluorescence reduced in the presence of 4NP ($7.5 \mu\text{M}$) up to 3 min. This quenching effect could be due to the interaction of the $-\text{COOH}$, $-\text{NH}_2$, and $-\text{SH}$ groups located on the NS-CDs' surface with 4NP. As soon as the reaction between 4NP and NS-CDs reached an equilibrium, no remarkable difference in the fluorescence intensity was noticed after 3 min. Hence, throughout the experiment, 3 min was taken as the favorable incubation time prior to taking the spectral measurements.

3.4 Sensitive detection of 4NP

To validate the sensitivity of this analytical method, under optimized experimental circumstances, the emission spectral features of NS-CDs were examined with respect to a series of uniformly increasing 4NP concentrations. Under the excitation of 350 nm, the emission spectra were measured in the wavelength range of 380–580 nm. As seen in Fig. 6, the fluorescence intensity of NS-CDs peaked at 465 nm and was steadily quenched with the concentration of 4NP increasing from $7.5 \mu\text{M}$. When the concentration attained $97.5 \mu\text{M}$, about 84% of the fluorescence intensity was reduced. Besides, the maximum quenching of NS-CDs by 4NP was visually verified under UV light irradiation ($\lambda_{UV}=365$ nm), where the strong cyan blue fluorescence color vanished (inset of Fig. 6). In Fig. 7, the calibration plot of fluorescence intensity (at 465 nm) versus 4NP concentration shows a linearity in the concentration range of 7.5 – $97.5 \mu\text{M}$ with

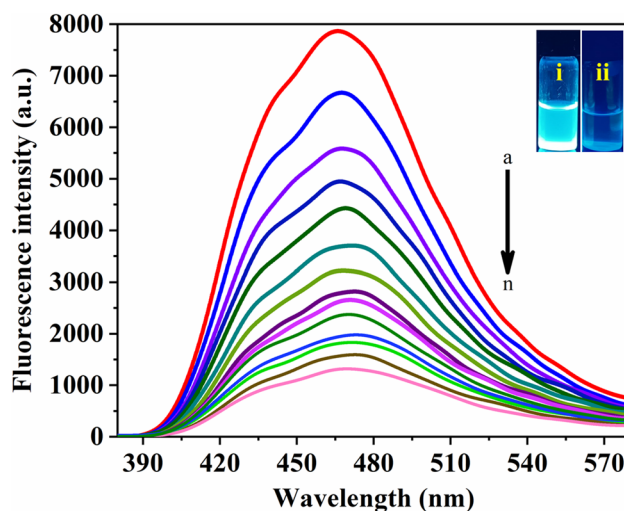


Fig. 6 Fluorescence spectral response of NS-CDs for different concentrations of 4NP analyte in water. a \rightarrow n represents the concentration of 4NP increasing from 0 to $97.5 \mu\text{M}$ in steps of $7.5 \mu\text{M}$ for each addition ($\lambda_{ex}=350$ nm and $\lambda_{em}=465$ nm). The insets are the photographs of (i) NS-CDs without 4NP and (ii) NS-CDs with $97.5 \mu\text{M}$ 4NP

a correlation coefficient of $R^2=0.9799$. The limit of detection (LOD) was determined from the equation, $\text{LOD}=3\sigma/m$, where σ means the standard deviation and m denotes the slope of the linear plot. The value of LOD was determined as $0.028 \mu\text{M}$ at a signal-to-noise ratio (SNR) of 3, which is lower than the EPA-recommended acceptable limit of 4NP in drinking water ($0.43 \mu\text{M}$). Furthermore, the sensing ability of C-CDs was examined by measuring the emission spectrum in the wavelength range of 350–550 nm under the excitation of 350 nm. As displayed in Fig. S5a, the emission intensity was centered at 417 nm while not reduced for the initial addition of 4NP ($10 \mu\text{M}$). However, the intensity was

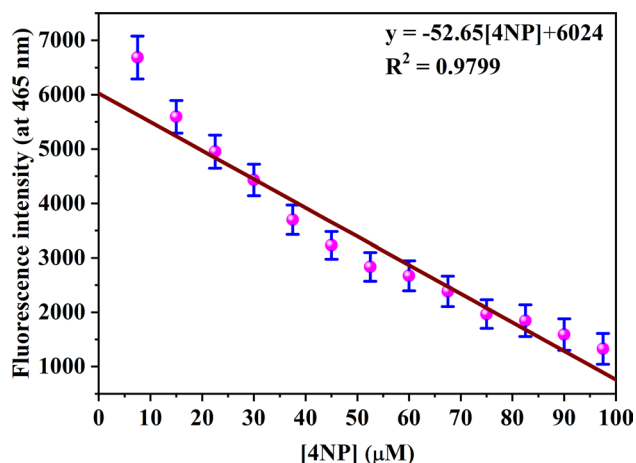


Fig. 7 Calibration plot for the fluorescence intensity of NS-CDs versus the concentration of 4NP

reduced for the 50 μM addition and this decreasing trend was continued up to 400 μM . Further increase of 4NP concentration did not produce any quenching effect and only 59% of fluorescence quenching was achieved for the final addition of 4NP (400 μM). In Fig. S5b, the calibration plot shows a linearity in the concentration range of 50–400 μM with a correlation coefficient of $R^2 = 0.9881$. The calculated

LOD was 2.29 μM , which was 82-fold less than the LOD value of NS-CDs (0.028 μM). This shows that C-CDs have much poorer sensing capability than NS-CDs. Hence, the proposed NS-CDs fluorescent probe is highly sensitive and can quantify 4NP at trace concentrations. A comparison of the as-developed probe with some already reported CD-based fluorescent probes for the 4NP determination is given in Table 1. As presented in Table 1, in terms of the linear range and LOD, the existing probe is analogous to/better than others.

3.5 Possible quenching mechanism

There are several pathways that could be feasible for the fluorescence quenching of NS-CDs such as photoinduced electron transfer (PET), Forster resonance energy transfer (FRET), excited-state reactions, IFE, SQ, dynamic quenching (DQ) [67]. For FRET and IFE processes, the condition of spectral overlap between the excitation band and/or emission band of the NS-CDs fluorescent probe and the absorption band of the 4NP analyte must be satisfied [68]. In the present work, as seen in Fig. 8a, the UV absorption spectrum of 4NP exhibits a broad spectral band in the range of 250–600 nm with an absorption maximum of 317 nm. Also, for the excitation at 350 nm, NS-CDs exhibit a strong emission

Table 1 Detection of 4NP using CDs as a fluorescent probe synthesized from various chemical precursors

Fluorescent probe	Chemical precursors	Linear range (μM)	LOD (μM)	Refs.
B,N co-doped CDs	3-Aminophenylboronic acid monohydrate	0.5–200	0.20	[52]
Molecularly imprinted polymers@CDs	Citric acid monohydrate + <i>o</i> -phenylenediamine	0–144	0.41	[53]
N,Si co-doped CDs	Diethylhexyl phthalate + N-[3-(Trimethoxysilyl)propyl]ethylenediamine	0.025–80	0.011	[54]
CDs	Celery leaves + L-glutathione	0.03–0.3	0.026	[55]
N-doped oxidized CDs	Citric acid + urea	2–2000	2	[56]
N-doped CDs	Hexamethylenetetramine + ethanediamine	0.5–70	0.201	[57]
N-doped CDs	β -Alanine + ethylene glycol	1–250	0.40	[58]
CDs	Sewage sludge	0.2–20	0.069	[59]
N,S co-doped CDs	Cuttlefish ink	0.05–125	0.039	[60]
CDs	Sweet flag (<i>Acorus calamus</i>)	0–14.28	0.207	[2]
N-CDs	<i>o</i> -Phenylenediamine + melamine	0.083–80	0.083	[61]
Silicon nanoparticles	N-[3-(trimethoxysilyl)propyl]ethylenediamine + <i>p</i> -aminophenol	0.5–60	0.074	[62]
CDs	Crayfish shells	0–50	0.16	[63]
Amine-functionalized perovskite quantum dots	Cesium bromide + Lead(II) bromide + 3-triethoxysilylpropylamine	0–3	0.16	[64]
Polyethyleneimine-based polymeric nanoparticles	Polyethyleneimine + formaldehyde + pyridoxal	5–50	0.42	[65]
Graphene quantum dots	Sea rice	0–1000	0.034	[66]
C-CDs	Citric acid	50–400	2.29	This work
NS-CDs	Citric acid + Cysteamine hydrochloride	7.5–97.5	0.028	

Bold significance highlight the importance of the present work

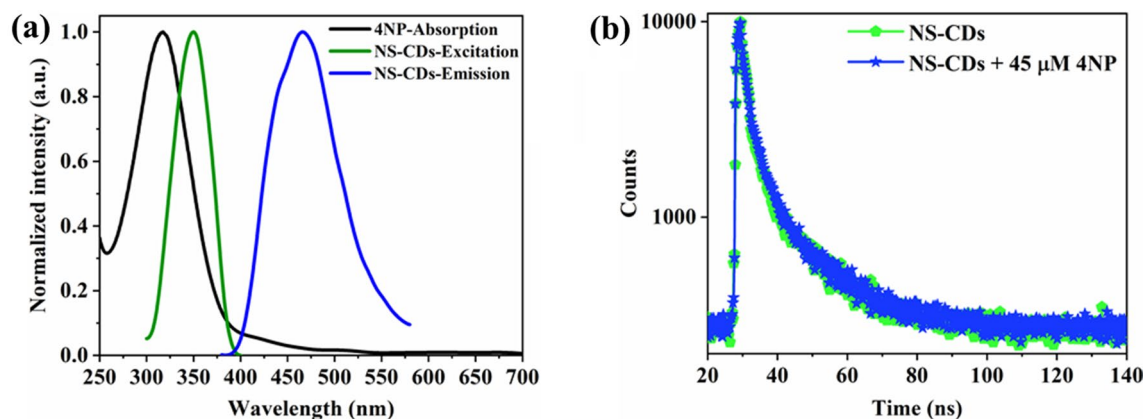


Fig. 8 **a** Spectral overlap of the UV absorption band of 4NP with the excitation band and the emission band of NS-CDs. **b** Fluorescence decay profile for NS-CDs without 4NP and with 4NP (45 μM) in water

maximum at 465 nm. The strong absorption band of 4NP well overlaps with the excitation band but scarcely with the emission band of NS-CDs, which opens up the possibility of the IFE process for fluorescence quenching (Fig. 8a).

To clarify further, the fluorescence decay time (τ) for NS-CDs before and after the 4NP addition was examined. The decay profiles were fitted by a single exponential function and the data is displayed in Fig. 8b. The decay time for NS-CDs without 4NP was 6.36 ns. After the 4NP addition (45 μM), the value was 6.21 ns. Since there is no significant change in the decay times, the chance for the FRET process can be excluded [2, 69]. Therefore, IFE would be the possible mechanism. However, there is a probability of PET between NS-CDs (donor) and 4NP (acceptor) for the fluorescence quenching, because NS-CDs have an electron-rich amino group (NH_2) and 4NP has an electron-deficient nitro-group [70].

Apart from this, other kinds of quenching mechanisms such as SQ and DQ can be conventionally defined by the Stern–Volmer equation [71],

$$\frac{F_0}{F} = 1 + K_{\text{SV}}[4\text{NP}] = 1 + K_q\tau[4\text{NP}], \quad (3)$$

where F_0 is the fluorescence intensity before the 4NP addition and F is the fluorescence intensity after the 4NP addition, K_{SV} is the Stern–Volmer quenching constant, $[4\text{NP}]$ is the 4-nitrophenol concentration, K_q is the bimolecular quenching rate constant, and τ is the fluorescence decay time of NS-CDs before the addition of 4NP. As defined by the above equation, the plot of F_0/F versus $[4\text{NP}]$ is presented in Fig. S6. It is clear that F_0/F shows a good linearity with the concentration of 4NP ranging from 7.5 to 97.5 μM . By taking the slope of the linear plot, the value of K_{SV} was found to be $4.410 \times 10^4 \text{ dm}^3 \text{ mol}^{-1}$. Substituting the value of τ (before the 4NP addition) in Equ. (3), K_q was obtained as

$6.933 \times 10^{12} \text{ dm}^3 \text{ mol}^{-1} \text{ s}^{-1}$. At this point, it is important to discuss the mechanism underlying the fluorescence quenching of NS-CDs by 4NP. The calculated value of K_q is much higher than the DQ constant ($2 \times 10^{10} \text{ dm}^3 \text{ mol}^{-1} \text{ s}^{-1}$), indicating the creation of a non-fluorescent ground-state complex (SQ) due to the interaction between the functional groups on NS-CDs' surface and 4NP [72, 73]. Das and Dutta verified a similar behavior in the quantification of 4NP using N-doped CDs [58]. In our work, the highly sensitive detection of 4NP by NS-CDs was possible due to the SQ process as well as IFE occurring between the NS-CDs probe and 4NP analyte. The C-CDs followed similar kinds of quenching mechanisms towards 4NP quantification, as displayed in Fig. S7. In addition to that, the QY was reduced to 7.5% for the final addition of 4NP (97.5 μM), which also supports the fluorescence quenching of NS-CDs.

3.6 Selectivity of 4NP detection

The selectivity of NS-CDs for the 4NP quantification was appraised by performing the fluorescence spectral studies on the NS-CDs with different interfering agents, such as phenol, *p*-phenylenediamine (pPD), 2-nitrotoluene (2NT), aniline, 4-nitroaniline (4NA), 4-chloroaniline (4CA), 4-bromophenol (4BP), 2-nitrophenol (2NP), 3-nitrophenol (3NP), 4-nitrobenzoic acid (4NBA), and hydroquinone (HQ) in the presence and absence of 4NP. The concentrations of 4NP and other interfering agents were taken as 100 μM each. The obtained results are presented as photographic images and bar diagrams in Fig. 9a, b. As seen in Fig. 9a, the response of NS-CDs to the abovementioned potential interfering agents in terms of fluorescence color change was examined under analogous experimental conditions. The NS-CDs displayed negligible fluorescence quenching response to the interfering

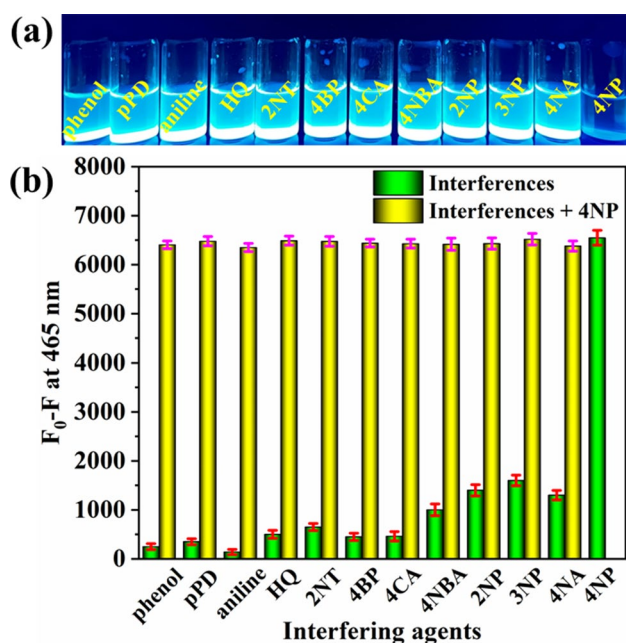


Fig. 9 a Photographs for NS-CDs with different interfering agents in UV light ($\lambda_{UV}=365$ nm). b Fluorescence response of NS-CDs to 4NP and selected interferences (100 μ M) in 100% aqueous medium. The green bars represent the responses of various interfering chemical compounds, whereas the yellow bars denote the responses of 4NP with various interferences

agents except for 4NP. Due to the introduction of 4NP into NS-CDs solution, the fluorescence of NS-CDs was efficiently reduced, while the intensity was almost unaffected by 2NT, 4NBA, 2NP, 3NP, and 4NA, which is displayed in Fig. 9b. No significant fluorescence quenching response was noticed for 2NP and 3NP because their absorption is less than 290 nm. Moreover, with the addition of 4NP to the NS-CDs solution containing other interferences, the fluorescence intensity of NS-CDs decreased, signifying that the present fluorimetric approach is highly selective to the 4NP sensing. As seen in Fig. S8, the selectivity of C-CDs was analyzed against the interfering compounds (400 μ M) and it showed fluorescence response against 2NP, 3NP, and 4NA. NS-CDs showed higher selectivity towards 4NP sensing than C-CDs. To summarize, NS-CDs were a potent fluorescent probe over C-CDs in terms of sensing ability and selectivity against potential interferences.

3.7 Detection in real water samples

As per the above results, the feasibility of NS-CDs for the quantitative determination of 4NP in real water samples was further explored by following the standard addition method. The obtained results are given in Table 2. As presented in Table 2, the analytical results showed that a trace of 4NP was not identified in the collected water samples. So, a recovery test was performed by sequentially adding the appropriate amount of 4NP (25 and 50 μ M) to the samples. Upon adding 4NP-spiked water samples with NS-CDs, the fluorescence intensity decreased, suggesting that 4NP solely affects the emission of NS-CDs. The recovery rate was in the range between 96.24 and 98.36% with a relative standard deviation (RSD) below 3.5%, representing there was no major interference in the real water samples by the addition of 4NP. These findings imply that the method is precise and reproducible, and it is possible to quantify 4NP in real water samples using the NS-CDs fluorescent probe.

4 Conclusions

A simple, non-toxic, and sensitive fluorescent probe was synthesized for the specific detection of trace 4NP in water using strong cyan blue emissive NS-CDs. The NS-CDs showed good fluorescence characteristics with a QY of about 52%. Under excitation at 350 nm, the NS-CDs exhibited a strong emission intensity centered at 465 nm. Emission intensity was reduced to about 84% for the final addition of 4NP analyte (97.5 μ M). Time-resolved fluorescence decay profile revealed that the IFE process occurring between NS-CDs and 4NP could account for fluorescence quenching, which led to an excellent 4NP sensing performance. The strong quenching was also accredited to the ground-state complex formation. Moreover, NS-CDs fluorescence-based detection of 4NP in water was not notably influenced by other nitro-substituted interfering agents in any manner. The NS-CDs achieved a LOD of 0.028 μ M for the detection of 4NP. The greater sensitivity and selectivity of NS-CDs over C-CDs ensured that NS-CDs can be a reliable fluorescent probe for quantifying trace 4NP in tap water and drinking water samples, with good recoveries.

Table 2 Quantification of 4NP in tap water and drinking water

Samples	4NP-spiked (μ M)	4NP-detected (μ M)	Recovery (%)	RSD (%) ($n=5$)
Tap water	25	24.23	96.92	1.81
	50	48.12	96.24	2.14
Drinking water	25	24.59	98.36	2.75
	50	48.74	97.48	1.56

Supplementary Information The online version contains supplementary material available at <https://doi.org/10.1007/s42823-023-00666-1>.

Acknowledgements This work was supported by the National Research Foundation of Korea (NRF) grant funded by the Korean government (MSIT) (no. NRF-2021M3H4A3A02086939) and also supported by the National Research Foundation of Korea (NRF) grant funded by the Korean government (MSIT) (no. RS-2023-00279149).

Author contributions KS: conceptualization, methodology, data curation, formal analysis, investigation, writing—original draft. RR: conceptualization, methodology, validation, investigation, visualization. HJ: validation, investigation, resources, writing—review and editing, visualization, supervision, funding acquisition.

Data availability All relevant data are available from the authors upon reasonable request.

Declarations

Conflict of interest The authors declare that they have no known competing financial interests or personal relationships that could have appeared to influence the work reported in this paper.

References

- Xiong Z, Zhang H, Zhang W, Lai B, Yao G (2019) Removal of nitrophenols and their derivatives by chemical redox: a review. *Chem Eng J* 359:13–31. <https://doi.org/10.1016/j.cej.2018.11.111>
- Venugopalan P, Vidya N (2023) Microwave assisted green synthesis of carbon dots from sweet flag (*Acorus calamus*) for fluorescent sensing of 4-nitrophenol. *J Photochem Photobiol A* 439:114625. <https://doi.org/10.1016/j.jphotochem.2023.114625>
- Khan KO, Assiri MA, Irshad H, Rafique S, Khan AM, Khan AK, Imran M, Shahzad SA (2023) Fluorescence based detection of industrially important and hazardous 4-Nitrophenol in real Samples: a combination of extensive optical and theoretical studies. *J Photochem Photobiol A* 442:114805. <https://doi.org/10.1016/j.jphotochem.2023.114805>
- Guo X, Li X, Jiang Y, Yi L, Wu Q, Chang H, Diao X, Sun Y, Pan X, Zhou N (2014) A spectroscopic study on the interaction between p-nitrophenol and bovine serum albumin. *J Lumin* 149:353–360. <https://doi.org/10.1016/j.jlumin.2014.01.036>
- Miletić AS, Pecev-Marinković ET, Grahovac ZM, Pavlović AN, Tošić SB, Mišić IDR (2019) Kinetic spectrophotometric method for 4-nitrophenol determination in drinking water. *J Anal Chem* 74:521–527. <https://doi.org/10.1134/S1061934819060066>
- Vilian AE, Choe SR, Giribabu K, Jang SC, Roh C, Huh YS, Han YK (2017) Pd nanospheres decorated reduced graphene oxide with multi-functions: Highly efficient catalytic reduction and ultrasensitive sensing of hazardous 4-nitrophenol pollutant. *J Hazard Mater* 333:54–62. <https://doi.org/10.1016/j.jhazmat.2017.03.015>
- Fischer J, Barek J, Wang J (2006) Separation and detection of nitrophenols at capillary electrophoresis microchips with amperometric detection. *Electroanalysis* 18:195–199. <https://doi.org/10.1002/elan.200503393>
- Almási A, Fischer E, Perjesi P (2006) A simple and rapid ion-pair HPLC method for simultaneous quantitation of 4-nitrophenol and its glucuronide and sulfate conjugates. *J Biochem Biophys Methods* 69:43–50. <https://doi.org/10.1016/j.jbbm.2006.05.002>
- Herterich R (1991) Gas chromatographic determination of nitrophenols in atmospheric liquid water and airborne particulates. *J Chromatogr A* 549:313–324. [https://doi.org/10.1016/S0021-9673\(00\)91442-0](https://doi.org/10.1016/S0021-9673(00)91442-0)
- Li F, Anjarsari Y, Wang J, Azzahidiah R, Jiang J, Zou J, Xiang K, Ma H, Arramel, (2023) Modulation of the lattice structure of 2D carbon-based materials for improving photo/electric properties. *Carbon Lett* 33:1321–1331. <https://doi.org/10.1007/s42823-022-00380-4>
- Liu F, Liu F, Qin Q, Zou J, Jiang J (2023) Relationship between the ^{13}C chemical shifts of adsorbed mesityl oxide and acid strength of solid acid catalysts. *Carbon Lett* 33:947–956. <https://doi.org/10.1007/s42823-023-00475-6>
- Zou J, Wu S, Liu Y, Sun Y, Cao Y, Hsu JP, Wee ATS, Jiang J (2018) An ultra-sensitive electrochemical sensor based on 2D g-C₃N₄/CuO nanocomposites for dopamine detection. *Carbon* 130:652–663. <https://doi.org/10.1016/j.carbon.2018.01.008>
- Jiang J, Ou-yang L, Zhu L, Zheng A, Zou J, Yi X, Tang H (2014) Dependence of electronic structure of g-C₃N₄ on the layer number of its nanosheets: a study by Raman spectroscopy coupled with first-principles calculations. *Carbon* 80:213–221. <https://doi.org/10.1016/j.carbon.2014.08.059>
- Zou J, Liao G, Jiang J, Xiong Z, Bai S, Wang H, Wu P, Zhang P, Li X (2022) In-situ construction of sulfur-doped g-C₃N₄/defective g-C₃N₄ isotope step-scheme heterojunction for boosting photocatalytic H₂ evolution. *Chin J Struct Chem* 41:2201025–2201033. <https://doi.org/10.14102/j.cnki.0254-5861.2021-0039>
- Yuan T, Meng T, He P, Shi Y, Li Y, Li X, Fan L, Yang S (2019) Carbon quantum dots: an emerging material for optoelectronic applications. *J Mater Chem C* 7:6820–6835. <https://doi.org/10.1039/C9TC01730E>
- Đorđević L, Arcudi F, Cacioppo M, Prato M (2022) A multifunctional chemical toolbox to engineer carbon dots for biomedical and energy applications. *Nat Nanotechnol* 17:112–130. <https://doi.org/10.1038/s41565-021-01051-7>
- Atchudan R, Edison TNJI, Lee YR (2016) Nitrogen-doped carbon dots originating from unripe peach for fluorescent bioimaging and electrocatalytic oxygen reduction reaction. *J Colloid Interface Sci* 482:8–18. <https://doi.org/10.1016/j.jcis.2016.07.058>
- Chauhan DS, Quraishi MA, Verma C (2022) Carbon nanodots: recent advances in synthesis and applications. *Carbon Lett* 32:1603–1629. <https://doi.org/10.1007/s42823-022-00359-1>
- Guo F, Zhu Z, Zheng Z, Jin Y, Di X, Xu Z, Guan H (2020) Facile synthesis of highly efficient fluorescent carbon dots for tetracycline detection. *Environ Sci Pollut Res* 27:4520–4527. <https://doi.org/10.1007/s11356-019-06779-3>
- Das D, Dutta RK (2022) Ethylene glycol and alanine anhydride based nitrogen doped fluorescent carbon nanoparticles as probe for detection of epinephrine, nor-epinephrine and dopamine. *Dyes Pigm* 203:110314. <https://doi.org/10.1016/j.dyepig.2022.110314>
- Chen Z, Zhou R, Cui J, Yan H, Li L (2021) Fabrication of fluorescent carbon dots by laser ablation in alkaline solution coupled with Ag nanoparticles for enhanced SERS. *MRS Commun* 11:489–497. <https://doi.org/10.1557/s43579-021-00060-w>
- Cui B, Yan L, Gu H, Yang Y, Liu X, Ma CQ, Chen Y, Jia H (2018) Fluorescent carbon quantum dots synthesized by chemical vapor deposition: an alternative candidate for electron acceptor in polymer solar cells. *Opt Mater* 75:166–173. <https://doi.org/10.1016/j.optmat.2017.10.010>
- Liu Y, Zhou Q, Yuan Y, Wu Y (2017) Hydrothermal synthesis of fluorescent carbon dots from sodium citrate and polyacrylamide and their highly selective detection of lead and pyrophosphate. *Carbon* 115:550–560. <https://doi.org/10.1016/j.carbon.2017.01.035>
- Liu Q, Zhang N, Shi H, Ji W, Guo X, Yuan W, Hu Q (2018) One-step microwave synthesis of carbon dots for highly sensitive

- and selective detection of copper ions in aqueous solution. *New J Chem* 42:3097–3101. <https://doi.org/10.1039/C7NJ05000C>
25. Saikia M, Singh A, Dihingia A, Khare P, Kalita J, Saikia BK (2022) Scalable production, cell toxicity assessment, and plant growth promotion activities of carbon quantum dots derived from low-quality coal feedstock. *Chem Eng J* 433:133633. <https://doi.org/10.1016/j.cej.2021.133633>
 26. Mintz KJ, Bartoli M, Rovere M, Zhou Y, Hettiarachchi SD, Paudyal S, Chen J, Domena JB, Liyanage PY, Sampson R, Khadka D (2021) A deep investigation into the structure of carbon dots. *Carbon* 173:433–447. <https://doi.org/10.1016/j.carbon.2020.11.017>
 27. Luo X, Zhang W, Han Y, Chen X, Zhu L, Tang W, Wang J, Yue T, Li Z (2018) N, S co-doped carbon dots based fluorescent “on-off-on” sensor for determination of ascorbic acid in common fruits. *Food Chem* 258:214–221. <https://doi.org/10.1016/j.foodchem.2018.03.032>
 28. Yang Z, Xu M, Liu Y, He F, Gao F, Su Y, Wei H, Zhang Y (2014) Nitrogen-doped, carbon-rich, highly photoluminescent carbon dots from ammonium citrate. *Nanoscale* 6:1890–1895. <https://doi.org/10.1039/C3NR05380F>
 29. Chandra S, Patra P, Pathan SH, Roy S, Mitra S, Layek A, Bhar R, Pramanik P, Goswami A (2013) Luminescent S-doped carbon dots: an emergent architecture for multimodal applications. *J Mater Chem B* 1:2375–2382. <https://doi.org/10.1039/C3TB00583F>
 30. Li H, Kong W, Liu J, Liu N, Huang H, Liu Y, Kang Z (2015) Fluorescent N-doped carbon dots for both cellular imaging and highly-sensitive catechol detection. *Carbon* 91:66–75. <https://doi.org/10.1016/j.carbon.2015.04.032>
 31. Pathak A, Chandhana JP, Ratheesh A, Nair BG, Suneesh PV, Babu TS (2021) Cysteamine derived N/S co-doped carbon dots for fluorescence imaging of pathogenic bacteria and human buccal epithelial cells. *Mater Lett* 305:130725. <https://doi.org/10.1016/j.matlet.2021.130725>
 32. Wang X, Zu X, Wang T, Zhao Y, Liang Y, Wang X, Chai Q, Zhang Y, Chen H, Wang H (2023) N, S-doped carbon dots prepared by peanut protein isolates and cysteamine as highly sensitive fluorescent sensors for Fe²⁺, Fe³⁺ and lactoferrin. *Polymers* 15:216. <https://doi.org/10.3390/polym15010216>
 33. Yang H, He L, Long Y, Li H, Pan S, Liu H, Hu X (2018) Fluorescent carbon dots synthesized by microwave-assisted pyrolysis for chromium(VI) and ascorbic acid sensing and logic gate operation. *Spectrochim Acta Part A* 205:12–20. <https://doi.org/10.1016/j.saa.2018.07.015>
 34. Yang M, Meng X, Li B, Ge S, Lu Y (2017) N, S co-doped carbon dots with high quantum yield: tunable fluorescence in liquid/solid and extensible applications. *J Nanopart Res* 19:217. <https://doi.org/10.1007/s11051-017-3914-7>
 35. Dai H, Shi Y, Wang Y, Sun Y, Hu J, Ni P, Li Z (2014) A carbon dot based biosensor for melamine detection by fluorescence resonance energy transfer. *Sens Actuators B* 202:201–208. <https://doi.org/10.1016/j.snb.2014.05.058>
 36. Rajamanikandan R, Shanmugaraj K, Ilanchelian M, Ju H (2023) Cysteamine-decorated gold nanoparticles for plasmon-based colorimetric on-site sensors for detecting cyanide ions using the smart-phone color ratio and for catalytic reduction of 4-nitrophenol. *Chemosphere* 316:137836. <https://doi.org/10.1016/j.chemosphere.2023.137836>
 37. Liang X, Zhang W, Zhang M, Qiu G, Zhang Y, Luo T, Kong C (2022) Facile synthesis of nitrogen-doped graphene quantum dots as nanocarbon emitters for sensitive detection of catechol. *RSC Adv* 12:25778–25785. <https://doi.org/10.1039/D2RA04209F>
 38. Tao R, Wang T, Fan J, Meyer HM III, Borisevich AY, Do-Thanh CL, Dai S (2022) Ionothermal synthesis of carbon/TiO₂ nanocomposite for supercapacitors. *Chem Nano Mat* 8:e202200075. <https://doi.org/10.1002/cnma.202200075>
 39. Yan F, Li J, Zhao X, Gong X (2023) Unveiling unconventional luminescence behavior of multicolor carbon dots derived from phenylenediamine. *J Phys Chem Lett* 14:5975–5984. <https://doi.org/10.1021/acs.jpcllett.3c01497>
 40. Jiang J, Xiong Z, Wang H, Liao G, Bai S, Zou J, Wu P, Zhang P, Li X (2022) Sulfur-doped g-C₃N₄/g-C₃N₄ isotope step-scheme heterojunction for photocatalytic H₂ evolution. *J Mater Sci Technol* 118:15–24. <https://doi.org/10.1016/j.jmst.2021.12.018>
 41. Jiang J, Bai S, Yang M, Zou J, Li N, Peng J, Wang H, Xiang K, Liu S, Zhai T (2022) Strategic design and fabrication of MXenes-Ti₃CNCl₂@CoS₂ core-shell nanostructure for high-efficiency hydrogen evolution. *Nano Res* 15:5977–5986. <https://doi.org/10.1007/s12274-022-4276-8>
 42. Xu D, Li M, Xu H, Yu J, Wang Y, Zhang P (2021) N, S-doped carbon quantum dots as a fluorescent probe for palladium(II) ions via Förster resonance energy transfer. *Results Chem* 3:100179. <https://doi.org/10.1016/j.rechem.2021.100179>
 43. Zhu S, Wang K, Hu J, Liu R, Zhu H (2020) Nitrogen and sulphur co-doped carbon quantum dots and their optical power limiting properties. *Mater Adv* 1:3176–3181. <https://doi.org/10.1039/D0MA00106F>
 44. Miao X, Yan X, Qu D, Li D, Tao FF, Sun Z (2017) Red emissive sulfur, nitrogen codoped carbon dots and their application in ion detection and theranostics. *ACS Appl Mater Interfaces* 9:18549–18556. <https://doi.org/10.1021/acsami.7b04514>
 45. Liang J, Wang Z, Huang L, Zou P, Liu X, Ni Q, Wang X, Wang W, Tao R (2023) Facile and tunable synthesis of nitrogen-doped graphene with different microstructures for high-performance supercapacitors. *ACS Mater Lett* 5:944–954. <https://doi.org/10.1021/acsmaterialslett.2c01092>
 46. Du K, Tao R, Guo C, Li H, Liu X, Guo P, Wang D, Liang J, Li J, Dai S, Sun XG (2022) In-situ synthesis of porous metal fluoride@carbon composite via simultaneous etching/fluorination enabled superior Li storage performance. *Nano Energy* 103:107862. <https://doi.org/10.1016/j.nanoen.2022.107862>
 47. Yang M, Chen Y, Wang H, Zou Y, Wu P, Zou J, Jiang J (2022) Solvothermal preparation of CeO₂ nanoparticles-graphene nanocomposites as an electrochemical sensor for sensitive detecting pentachlorophenol. *Carbon Lett* 32:1277–1285. <https://doi.org/10.1007/s42823-022-00353-7>
 48. Chen Y, Tu C, Liu Y, Liu P, Gong P, Wu G, Huang X, Chen J, Liu T, Jiang J (2023) Microstructure and mechanical properties of carbon graphite composites reinforced by carbon nanofibers. *Carbon Lett* 33:561–571. <https://doi.org/10.1007/s42823-022-00445-4>
 49. Pooja D, Saini S, Thakur A, Kumar B, Tyagi S, Nayak MK (2017) A “Turn-On” thiol functionalized fluorescent carbon quantum dot based chemosensory system for arsenite detection. *J Hazard Mater* 328:117–126. <https://doi.org/10.1016/j.jhazmat.2017.01.015>
 50. Shi W, Guo F, Han M, Yuan S, Guan W, Li H, Huang H, Liu Y, Kang Z (2017) N, S co-doped carbon dots as a stable bio-imaging probe for detection of intracellular temperature and tetracycline. *J Mater Chem B* 5:3293–3299. <https://doi.org/10.1039/C7TB00810D>
 51. Dong Y, Pang H, Yang HB, Guo C, Shao J, Chi Y, Li CM, Yu T (2013) Carbon-based dots co-doped with nitrogen and sulfur for high quantum yield and excitation-independent emission. *Angew Chem Int Ed* 52:7800–7804. <https://doi.org/10.1002/anie.201301114>
 52. Xiao N, Liu SG, Mo S, Li N, Ju YJ, Ling Y, Li NB, Luo HQ (2018) Highly selective detection of p-nitrophenol using fluorescence assay based on boron, nitrogen co-doped carbon dots. *Talanta* 184:184–192. <https://doi.org/10.1016/j.talanta.2018.02.114>

53. Wang K, Tan L, Zhang Y, Zhang D, Wang N, Wang J (2023) A molecular imprinted fluorescence sensor based on carbon quantum dots for selective detection of 4-nitrophenol in aqueous environments. *Mar Pollut Bull* 187:114587. <https://doi.org/10.1016/j.marpolbul.2023.114587>
54. Wang X, Liu Y, Wang Q, Bu T, Sun X, Jia P, Wang L (2021) Nitrogen, silicon co-doped carbon dots as the fluorescence nano-probe for trace p-nitrophenol detection based on inner filter effect. *Spectrochim Acta Part A* 244:118876. <https://doi.org/10.1016/j.saa.2020.118876>
55. Qu Y, Yu L, Zhu B, Chai F, Su Z (2020) Green synthesis of carbon dots by celery leaves for use as fluorescent paper sensors for the detection of nitrophenols. *New J Chem* 44:1500–1507. <https://doi.org/10.1039/C9NJ05285B>
56. Bogireddy NKR, Silva RC, Valenzuela MA, Agarwal V (2020) 4-nitrophenol optical sensing with N doped oxidized carbon dots. *J Hazard Mater* 386:121643. <https://doi.org/10.1016/j.jhazmat.2019.121643>
57. Liao S, Ding Z, Wang S, Tan F, Ge Y, Cui Y, Tan N, Wang H (2021) Fluorescent nitrogen-doped carbon dots for high selective detecting p-nitrophenol through FRET mechanism. *Spectrochim Acta Part A* 259:119897. <https://doi.org/10.1016/j.saa.2021.119897>
58. Das D, Dutta RK (2021) N-doped carbon dots synthesized from ethylene glycol and β -alanine for detection of Cr(VI) and 4-nitrophenol via photoluminescence quenching. *ACS Appl Nano Mater* 4:3444–3454. <https://doi.org/10.1021/acsnm.0c03329>
59. Hu Y, Gao Z (2020) Sewage sludge in microwave oven: a sustainable synthetic approach toward carbon dots for fluorescent sensing of para-Nitrophenol. *J Hazard Mater* 382:121048. <https://doi.org/10.1016/j.jhazmat.2019.121048>
60. Huang X, Yang C, Chen Y, Zhu Z, Zhou L (2021) Cuttlefish ink-based N and S co-doped carbon quantum dots as a fluorescent sensor for highly sensitive and selective para-nitrophenol detection. *Anal Methods* 13:5351–5359. <https://doi.org/10.1039/D1AY01496J>
61. Guo G, Zheng Q, Li T, Zhang T, Tang S, Li L, Gao S, Tang Y, Chen D (2023) 3D printed self-calibrating on-site sensing platform based on bimodal excitation carbon dots for visual 4-nitrophenol detection by means of the localization of inner filter effect and pH regulation. *Chem Eng Sci* 281:119201. <https://doi.org/10.1016/j.ces.2023.119201>
62. Liu F, Liang F, Li Z, Kang G, Wang T, Chen C, Lu Y (2023) Fluorescence detection of 4-nitrophenol and α -glucosidase activity based on 4-nitrophenol-regulated fluorescence of silicon nanoparticles. *Analyst* 148:4030–4036. <https://doi.org/10.1039/D3AN00966A>
63. Chen J, Xia X, Li P, Yu H, Xie Y, Guo Y, Yao W, Qian H, Cheng Y (2023) Crayfish shells-derived carbon dots as a fluorescence sensor for the selective detection of 4-nitrophenol. *Food Agric Immunol* 34:36–47. <https://doi.org/10.1080/09540105.2022.2139358>
64. Lin YC, Lin PY, Beck DE, Hsu YC, Cheng SH, Hsieh S (2023) Fluorescence quenching detection of p-nitrophenol in river water using functional perovskite quantum dots. *Environ Technol Innov* 32:103297. <https://doi.org/10.1016/j.eti.2023.103297>
65. Saini AK, Jali BR, Sahoo SK (2023) Polyethyleneimine-based fluorescent polymeric nanoparticles: synthesis and application in fluorescence sensing of pH and para-nitrophenol. *New J Chem* 47:9250–9256. <https://doi.org/10.1039/D3NJ01508D>
66. Luo K, Luo X, Wu Y, Liang Z, Kang X, Wen Y (2023) Synthesis of graphene quantum dots with temperature-sensitive properties from sea rice for rapid and highly selective detection of 4-nitrophenol. *Diamond Relat Mater* 135:109849. <https://doi.org/10.1016/j.diamond.2023.109849>
67. Zu F, Yan F, Bai Z, Xu J, Wang Y, Huang Y, Zhou X (2017) The quenching of the fluorescence of carbon dots: a review on mechanisms and applications. *Microchim Acta* 184:1899–1914. <https://doi.org/10.1007/s00604-017-2318-9>
68. Tang J, Zhang Y, Liu Y, Liu D, Qin H, Lian N (2019) Carbon quantum dots as a fluorophore for “inner filter effect” detection of metronidazole in pharmaceutical preparations. *RSC Adv* 9:38174–38182. <https://doi.org/10.1039/C9RA08477K>
69. Wang M, Shi R, Gao M, Zhang K, Deng L, Fu Q, Wang L, Gao D (2020) Sensitivity fluorescent switching sensor for Cr (VI) and ascorbic acid detection based on orange peels-derived carbon dots modified with EDTA. *Food Chem* 318:126506. <https://doi.org/10.1016/j.foodchem.2020.126506>
70. Yang X, Wang D, Luo N, Feng M, Peng X, Liao X (2020) Green synthesis of fluorescent N, S-carbon dots from bamboo leaf and the interaction with nitrophenol compounds. *Spectrochim Acta Part A* 239:118462. <https://doi.org/10.1016/j.saa.2020.118462>
71. Rajamanikandan R, Ilanchelian M, Ju H (2023) Highly selective uricase-based quantification of uric acid using hydrogen peroxide sensitive poly-(vinylpyrrolidone) templated copper nanoclusters as a fluorescence probe. *Chemosensors* 11:268. <https://doi.org/10.3390/chemosensors11050268>
72. Rajamanikandan R, Aazaad B, Lakshminpathi S, Ilanchelian M (2020) Glutathione functionalized copper nanoclusters as a fluorescence platform for specific biosensing of cysteine and application in cellular imaging. *Microchem J* 158:105253. <https://doi.org/10.1016/j.microc.2020.105253>
73. Ashokan I, Bhunia SK (2023) Boron and nitrogen co-doped bright yellow fluorescent carbon dots as real-time selective detection of phthalic acid plasticizer in aqueous medium. *J Photochem Photobiol A* 437:114489. <https://doi.org/10.1016/j.jphotochem.2022.114489>

Publisher's Note Springer Nature remains neutral with regard to jurisdictional claims in published maps and institutional affiliations.

Springer Nature or its licensor (e.g. a society or other partner) holds exclusive rights to this article under a publishing agreement with the author(s) or other rightsholder(s); author self-archiving of the accepted manuscript version of this article is solely governed by the terms of such publishing agreement and applicable law.